

Section 1

PROGRESS ON OMEGA

1.A OMEGA Activation

The principal activity on OMEGA during the last quarter was the installation of components in the target area and the initiation of 2 and 6 beam target calibration shots. These experiments are designed to test the laser beam pointing and focusing on spherical microballoon targets with each of the 24 beams. The diagnostics employed for these tests consisted of two x-ray pinhole cameras to provide spatially resolved photographs of the x-ray emission from the target.

The OMEGA 24 beam neodymium phosphate glass laser system ($\lambda=1.054\mu\text{m}$) performance tests were reported in a previous issue of the LLE Review (Volume 2). The OMEGA system design features allow the high repetition rate of one shot every 30 minutes at a power level of 12 TW for a pulse length of 50 psec.

Table 1
The principal objectives and results from the OMEGA laser system performance test.

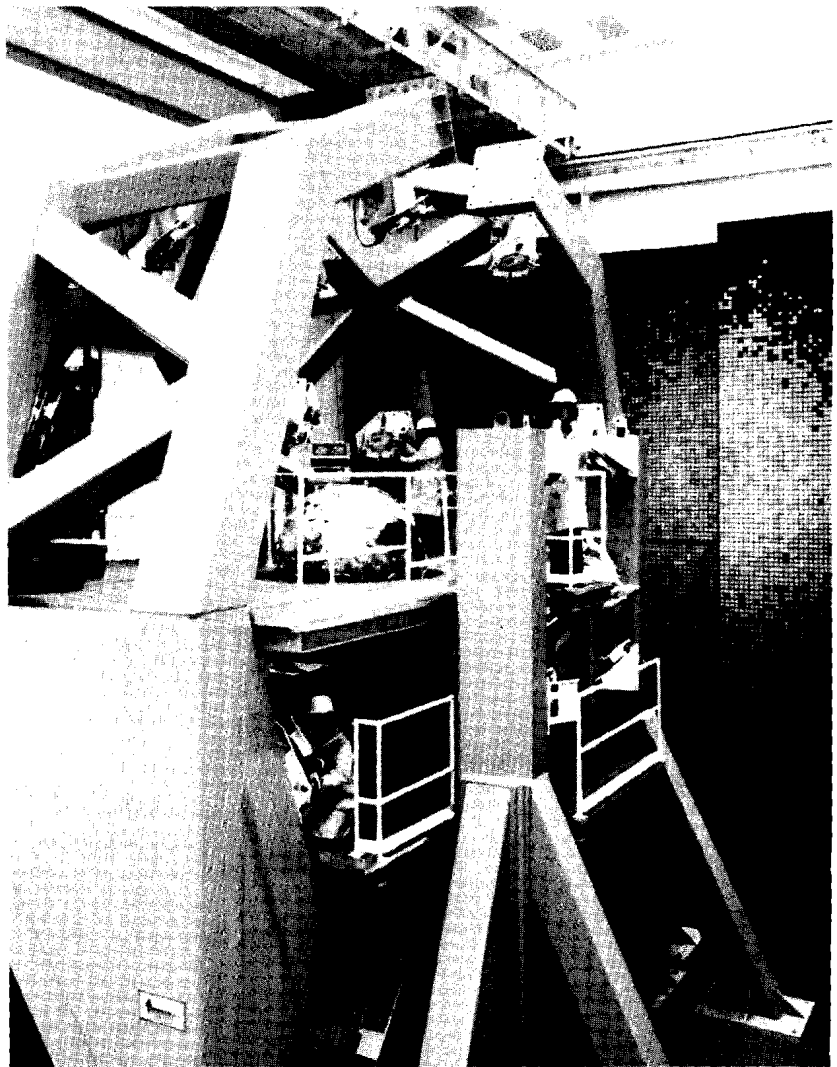
	Minimum DOE Requirements	Design Goal	OMEGA Output (1/80)
Peak Power (short pulse)	7.5 TW (50 psec)	12-14 TW (50 psec)	12.2 TW (53 psec)
Energy (long pulse)	1.2 kJ (300 psec)	2.5 kJ (300 psec)	1.76 kJ (273 psec)

The principal objectives and results from the performance tests are summarized in Table 1. Further details of these tests can be found in the LLE Review, Volume 2.

The OMEGA target area is shown in Figure 1; the large structure supports the final turning mirrors for directing 24 beams to the target chamber and focusing lenses. The activities during the last quarter consisted of assembly of components in the target area including optics, target chamber support equipment, and diagnostics. The following major components have been installed and tested:

1. All optical mirrors and covers were installed on the turning mirror structure.
2. 17 of the 24 single element f/3 focusing lenses were installed in the target chamber.
3. The target chamber vacuum system was tested and obtained a pressure of 5×10^{-7} torr.

Figure 1
Photograph of the OMEGA target area showing the turning mirror support structure and experimental chamber.



4. The target positioner, capable of holding up to 16 targets, was placed on the target chamber.
5. The target chamber viewing system, for positioning of targets, was installed.

Additional construction activities included the OMEGA diagnostic control room for data acquisition and the fabrication of diagnostic systems which included 20 plasma calorimeters for absorbed energy measurements, two x-ray pinhole cameras for spatial x-ray imaging, and neutron counters.

During the quarter, 17 target shots were taken on the OMEGA facility. These first series of target shots were designed to test the pointing, focusing, and timing of the OMEGA illumination system. The test results are obtained by irradiating an empty glass microballoon of 200 μm diameter and a 2.0 μm glass wall with two and six beams. X-ray images of the plasma emission are obtained from an x-ray pinhole camera and compared with the predicted results. A typical experiment with 2 beams focused on the target surface shows three well-defined x-ray images in a straight line; the outer images are the result of localized plasma heating from the focused beam energy; the center image is due to the two colliding glass segments stagnating at target center. Gross errors in beam timing are observed if the central x-ray image is displaced from target center. The location of beam focusing is compared with predicted results by similar experiments which translate the beam focus from inside to outside the target surface. This focusing change should result in a larger x-ray image than that obtained with a surface focus condition.

1.B OMEGA Beam Propagation

OMEGA utilizes the imaging property of its spatial filters to relay an image of a hard aperture, located at the output of the oscillator, through each of its amplifiers. This concept, first proposed by John Hunt at LLNL, allows the system to be operated at a high fill factor and minimizes diffraction effects that can lead to beam breakup and subsequent catastrophic damage of optical components in the system. The last image plane in OMEGA is located approximately 2 meters beyond the output spatial filter in each of the 24 beamlines. Each beam propagates from this plane to the target chamber focusing lens without additional spatial filtering or image relaying. The total unrelayed optical path for each beam is approximately 30 meters. The presence of this large unrelayed optical path has been a cause for concern regarding the beam quality at the focusing lens.

An additional cause for concern is the fact that the beams are unenclosed over the 30 meter path between the output of the

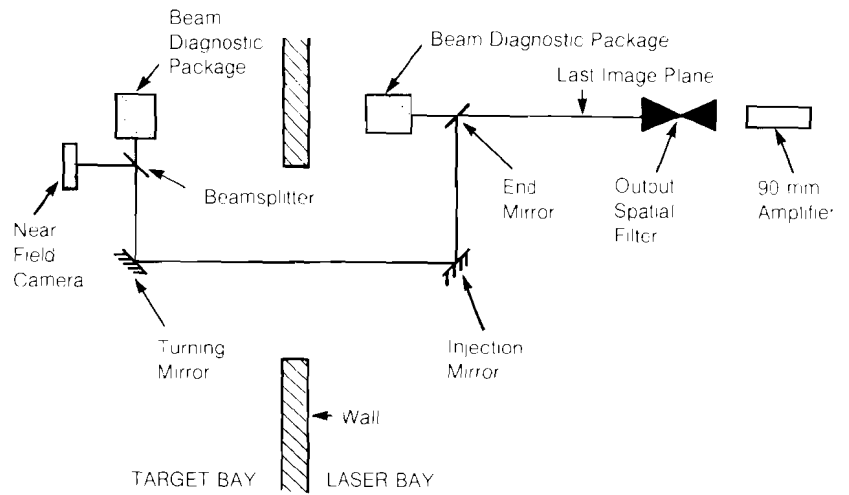


Figure 2
Laser beam path from system output.

laser system and the focusing lens. This has led to speculation that the beam quality would be substantially degraded by air turbulence in the laser and target bays. Experience at LLNL suggested that beam enclosures would be necessary; however, the air conditioning systems at the Shiva and OMEGA facilities are of considerably different design.

A preliminary series of experiments has been conducted to determine the magnitude of these potential problems. The problem of beam quality degradation was addressed by photographing the far field distribution of a single beam in the laser bay and near the target chamber using the standard OMEGA beam diagnostic package (BDP).

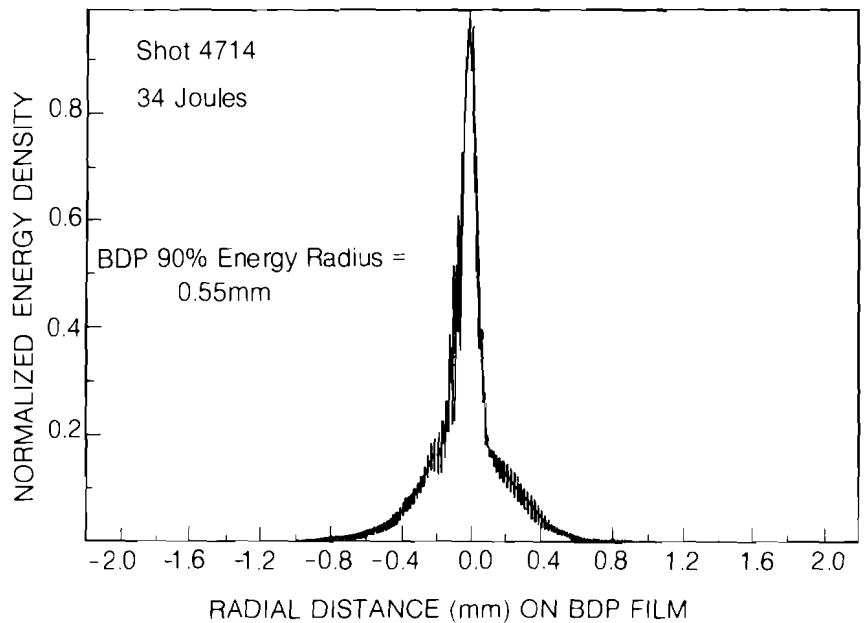


Figure 3
Laser bay far field beam profile.

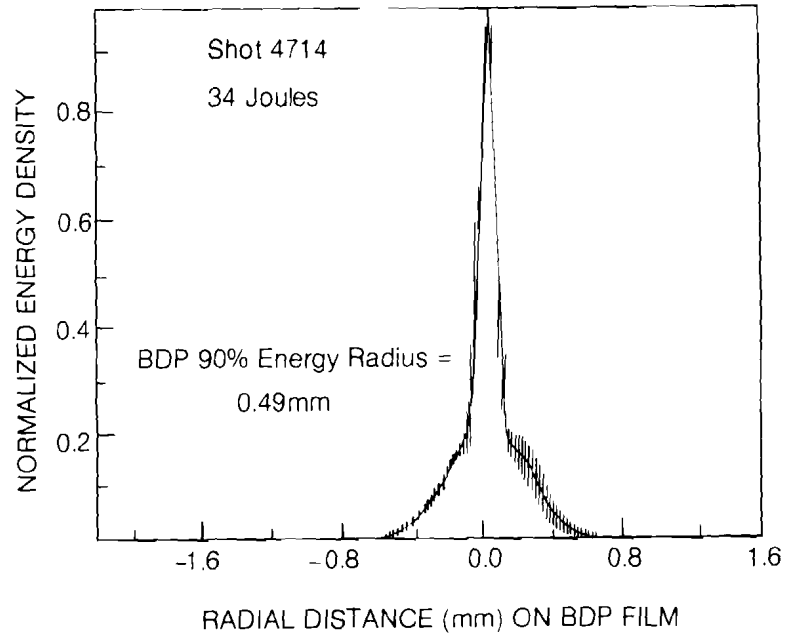
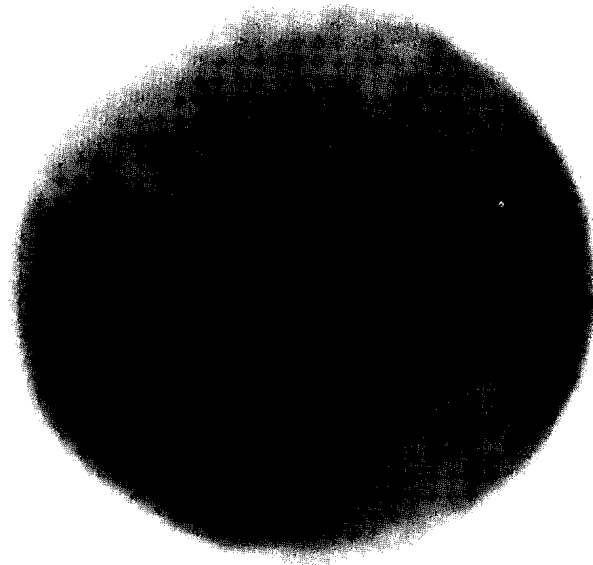


Figure 4
Target bay far field beam profile.

The BDP uses a 4.5 meter focal length lens to produce a photograph of the beam at the equivalent target plane on 35mm film. Experience with ZETA has shown that there is a high correlation between the BDP equivalent target plane photographs and the x-ray emission as seen in pinhole camera photographs of gold coated targets. Thus, the BDP can be used as a diagnostic to determine on-target beam quality.

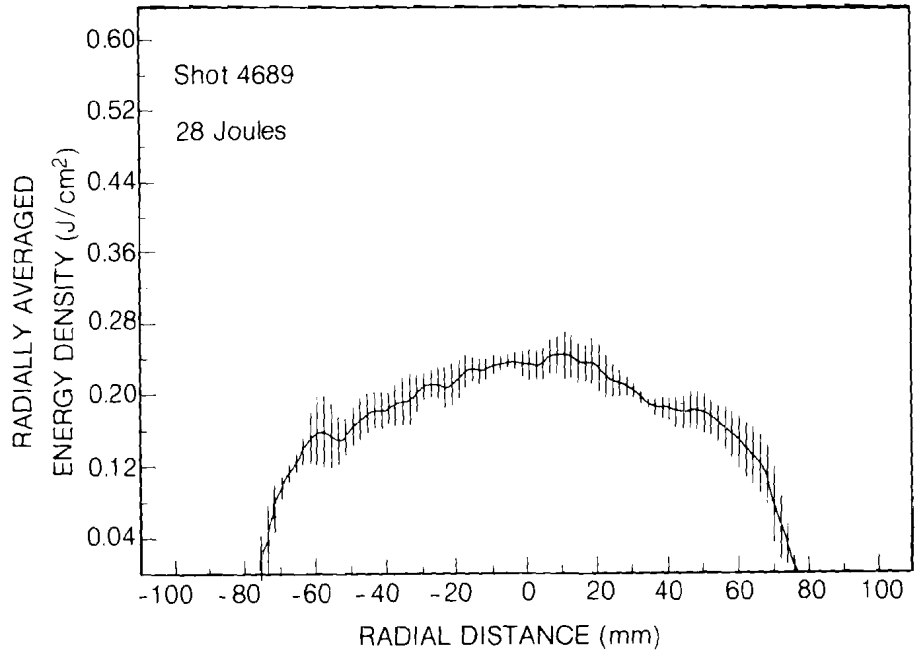
The problem of diffraction and beam breakup was addressed in a separate experiment using a near field photograph taken in a

Figure 5
Near field photograph of an
OMEGA beam in the target bay.



Shot 4689

Figure 6
Target bay near field beam profile.



plane near the final focusing lens. Significant modulation of the beam intensity profile in this plane can result in damage of the focusing lens. Figure 2 illustrates the arrangement of equipment for each of these experiments.

Figure 3 shows the average of 4 radial scans of the far field photograph taken in the laser bay. Figure 4 shows the average of 4 radial scans of the far field photo taken in the target bay. Figure 5 is a near field photograph of the beam taken near the OMEGA chamber and Figure 6 is an average of four radial scans of the near field photo.

The following conclusions can be drawn from these photographs:

1. The similarity of the BDP far field photographs taken in the laser bay and the target bay indicates that there is no significant change in focusing characteristics due to air turbulence or the lack of image relaying over the 30 meter path.
2. The lack of significant modulation in the near field photograph in the target bay indicates that the beam arrives at the chamber without breaking-up despite the lack of image relaying, thus damage of the focusing optics is unlikely.

It should be emphasized that these are preliminary measurements, and additional experiments are planned in an effort to further understand the propagation of these high energy beams. These experiments will be useful in normalizing propagation codes, which will then be used to enhance the performance of OMEGA.

1.C Uniformity of Illumination Studies for OMEGA

Arranging the distribution of irradiation on the surface of spherical targets as uniformly as possible is an important goal for laser

fusion. A multi-beam symmetric irradiation capability is one of the distinct features of the OMEGA facility. It is expected that the more uniform the distribution of irradiation, the more uniform will be the temperature on the target surface, resulting in higher compression and implosion quality.

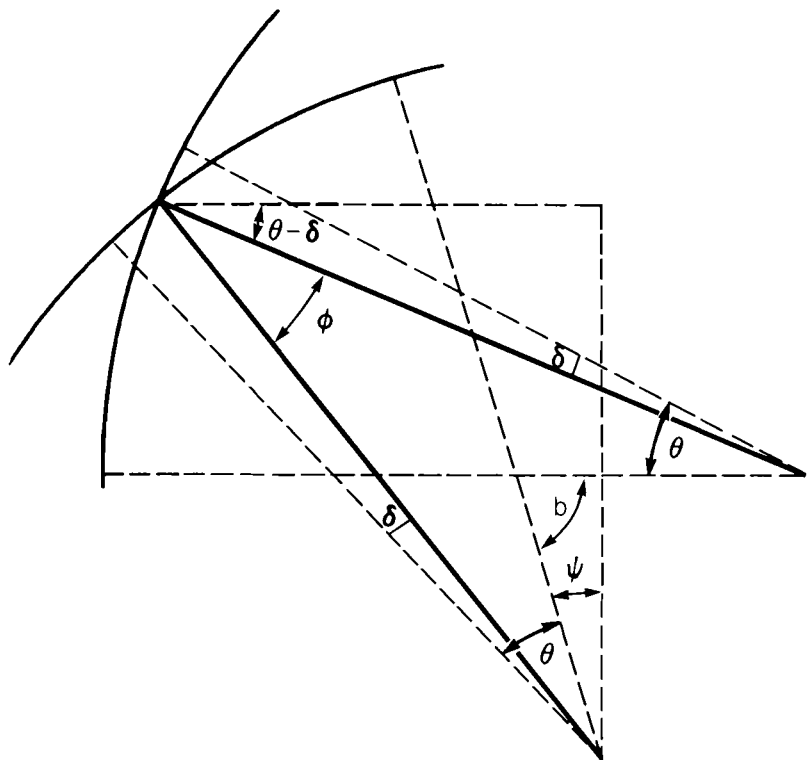
We summarize our present results from studies of the achievable uniformity to be expected on OMEGA.

In principle, and under ideal situations, the irradiation of spherical targets by laser beams might be expected to result in complete uniformity of irradiance. Here we restate the result that absolute uniformity on a spherical target is not attainable, even in principle.

G. Birkhoff¹ has shown that there exists only one spherically symmetric source-free solution of Einstein's field equations (Schwarzschild solution) which is static (i.e., field variables are independent of time). This is known as Birkhoff's theorem. Birkhoff's theorem has since been generalized² and, when applied to electromagnetic radiation, states that electromagnetic radiation cannot be truly spherically symmetric. This can also be shown in a more familiar way (e.g., see Jackson^{3,4}).

First, consider a segment of a "spherical wave" focused at the target center with a finite coherence time τ_c equal to the pulse-width. It can be shown⁵ that the normalized autocorrelation (or

Figure 7
 Geometry illustrating the angle ϕ between the rays from two lenses, each of half-angle θ . The beam axes form an angle b with respect to each other. The optical axis of each beam is assumed to pass through the target center. The angle δ selects any ray between $\delta = \theta$ (on-axis ray) to $\delta = 0$ (marginal ray) for each ray pair considered.



mutual coherence) function $\gamma(\vec{r}_1, \vec{r}_2, \tau)$ changes very slowly over any part of the target surface. Moreover, the cosine phase term will change rapidly because of the presence of the phase difference which is inversely proportional to the wavelength⁵. Thus over a portion of the target surface (such as the region covered by one beam), the average intensity will have negligible nonuniformity. In other words, the interference effect due to finite temporal coherence for a "spherical wave" on a spherical target approaches zero. Thus, we are justified in assuming perfect temporal coherence as far as illumination uniformity is concerned.

When a spherical target is irradiated by n monochromatic beams, the interference fringes in the overlapping region of the beams have the following characteristics:

1. The angle between two rays (or wavefronts) from any two beams is quite large. This can be seen from Figure 7. b and ϕ are angles between two beam axes and two rays respectively, and θ is the lens half-angle. From Figure 7, it is clear that $b + \Psi = \phi + 2(\theta - \delta) + \Psi$ or $\phi = b - 2(\theta - \delta)$. Thus, $\phi_{\min} = b - 2\theta$. For the ZETA system, $b = 90^\circ$, $\theta = 22.5^\circ$, and $\phi_{\min} = 45^\circ$. With such a large angle, the spacing between fringes is given by $d = \lambda / \sin 45^\circ = 1.4\lambda$, which is of the order of one wavelength.
2. The contrast between "bright" and "dark" interference fringes between any two beams is quite small for the six-beam ZETA system and not very large for the 24-beam OMEGA system due to the fact that the angle between two wavefronts is about 45° for ZETA and 28° for OMEGA. The contrast for multi-beam interference fringes will be even smaller.
3. Lens aberrations will further suppress the importance of interference fringes due to multiple beams⁶.

Consequently, the interference fringes in the overlapping region are negligible.

Initially, the focused electromagnetic field in spherical geometry was treated in terms of Debye potentials⁷. The treatment of electromagnetic waves in a dense spherically symmetric plasma enables the matching of boundary conditions of tangential and normal components of \vec{E} and \vec{B} . The treatment is very similar to Erkkila's dissertation⁸ except that ponderomotive force effects and filamentation are also considered in addition to inverse bremsstrahlung and resonance absorption processes.

However, if diffraction is to be considered, then rigorous diffraction theory has to be applied, which is a major unsolved problem in itself. Fortunately, it has been established^{9,10} that even in a large aperture spherical system [typically the angular semi-aperture (lens half-angle) can be up to 40°] scalar diffraction theory is still valid for describing the image field. Because the

ZETA and OMEGA systems use lenses of $f/1.2$ and $f/3$, with lens half-angles of 22.5° and 9° respectively, scalar diffraction theory is sufficient for our discussion of target irradiance for both systems.

Before proceeding with a detailed description of our latest results, a short summary of previous preliminary calculations performed (1976 to 1978) on the uniformity of illumination achievable on spherical targets for both the ZETA and OMEGA systems will be presented. This earlier work considered geometric optics with several intensity profiles and artificial absorption coefficient models which we shall discuss shortly.

The uniformity of illumination on a spherical target depends on the disposition of the beams, whole angle (or $f/\#$) of the lens, focal position of the lenses, radial intensity profiles of the beam, absorption coefficients of the target, and any target misalignment error.

Leppelmeier¹¹ and Howard¹³ have shown the necessity of using fast lens in order to obtain uniformity of illumination on a spherical target. This work^{11, 13} included the effects of different numbers of beams and their disposition. The number of beams,

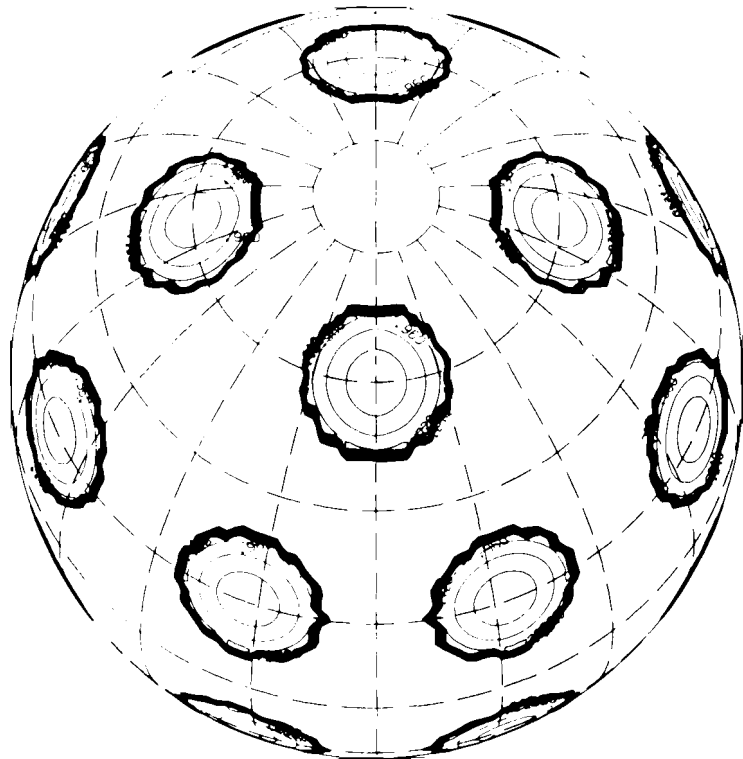


Figure 8

On target intensity contour plot from the OMEGA system for a reverse quadratic intensity profile (ratio = 0.2, focus = 0.2).

Contour from 0.0 to 0.96 (Contour Interval of 0.06)

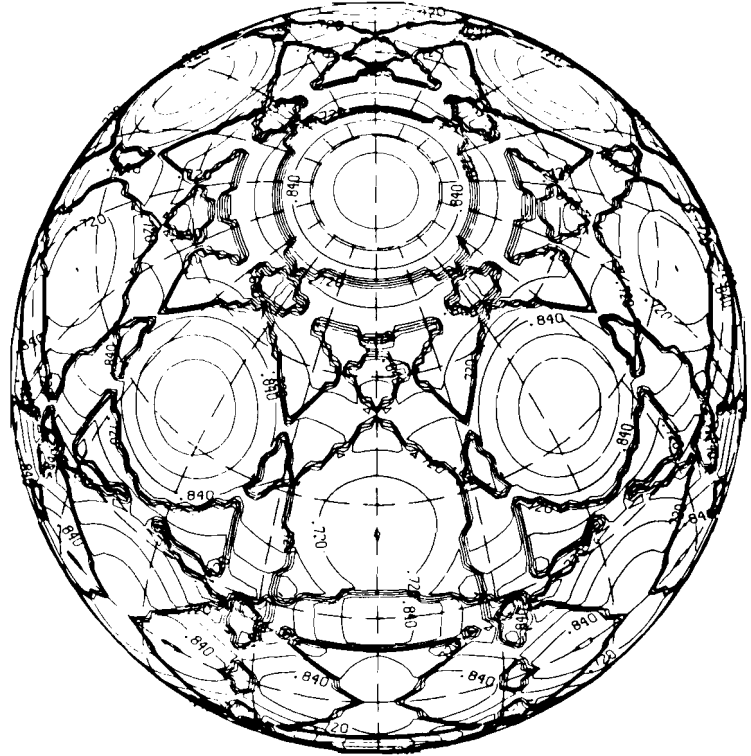


Figure 9
On target intensity contour plot from the OMEGA system for a reverse quadratic intensity profile (ratio = 0.2, focus = 3.6).

Contour from 0.48 to 0.99 (Contour Interval of 0.03)

their geometrical arrangement, and the $f/\#$ of the lenses for both ZETA and OMEGA were decided based upon Leppelmeier's work; the work by Lee¹² was to determine how the uniformity of illumination depends on the remaining parameters.

In the preliminary simulations, different beam radial intensity profiles were considered:

1. Flat top $I(r) = I_0$,
2. Quadratic $I(r) = I_0[1-(r/R)^2]$,
3. Soft-supergaussian $I(r) = I_0 \exp[-a(r/R)^5]$,
4. Reversed quadratic $I(r) = I_0 [1-\text{ratio} (1-(r/R)^2)]$ with different depth to height ratios from 0.1 to 0.5.

Although many of the relevant absorption processes are qualitatively understood, the quantitative distribution of each process is not known. Thus in these studies different mixes of the various absorption coefficients appropriate to different absorption mechanisms have been considered. Results for a few mixed "legislated" absorption coefficients, which represent an approximation of experimentally observed values for the various processes, will be presented below. Nonuniformity in terms of the percentage of σ/\bar{I} is plotted against the focal position in terms of target radii behind the target center for each absorption coefficient, where σ is the RMS deviation of the intensity and \bar{I} is the mean intensity. An acceptable level of nonuniformity of target illumination (σ/\bar{I}) is assumed to be less than 10%.

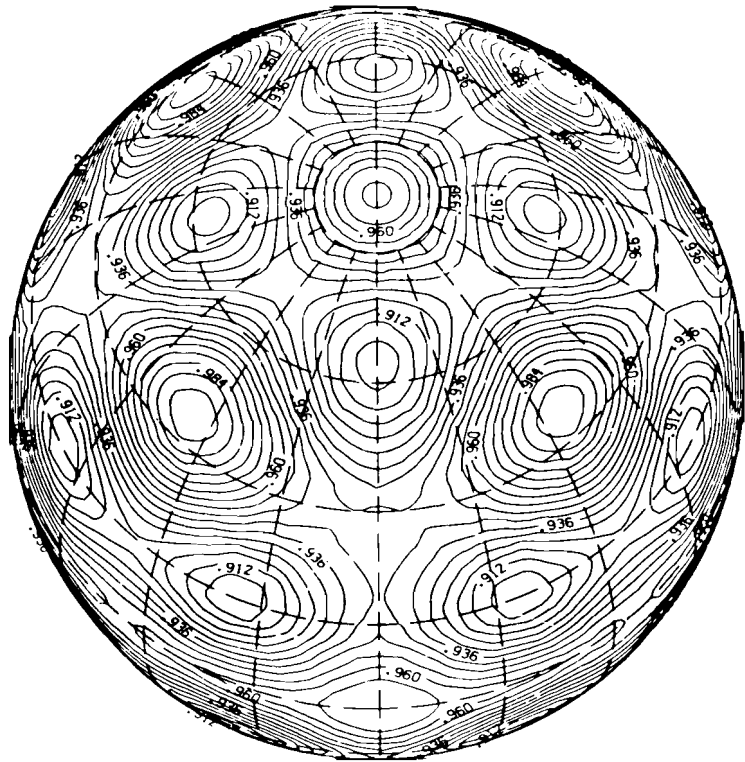


Figure 10
 On target intensity contour plot from the OMEGA system for a reverse quadratic intensity profile (ratio = 0.2, focus = 5.6).

Contour from 0.894 to 0.996 (Contour Interval of 0.006)

Recently, longer pulsewidth and longer plasma scale lengths, together with conditions appropriate for $3\omega_0$ ("blue") irradiation experiments, have been considered. Contour plots of the intensity distribution on target, as well as plots of intensity at constant latitude θ and longitude ϕ have been implemented. Figures 8 through 10 display contours of the intensity distribution on a target

Reverse Quadratic Intensity Profile
 Ratio = 0.20

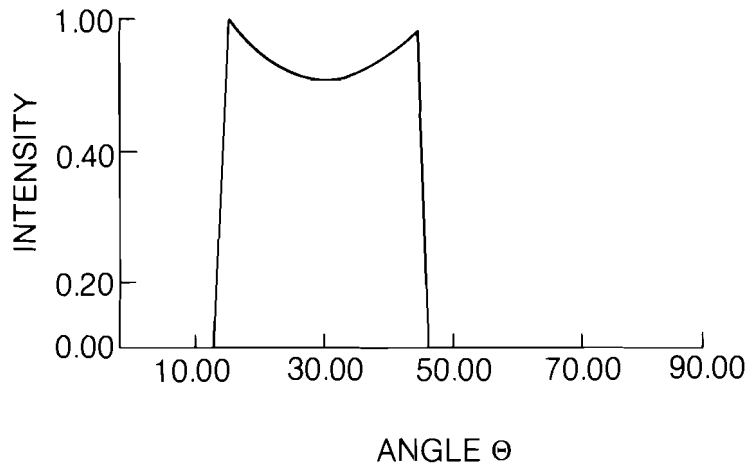
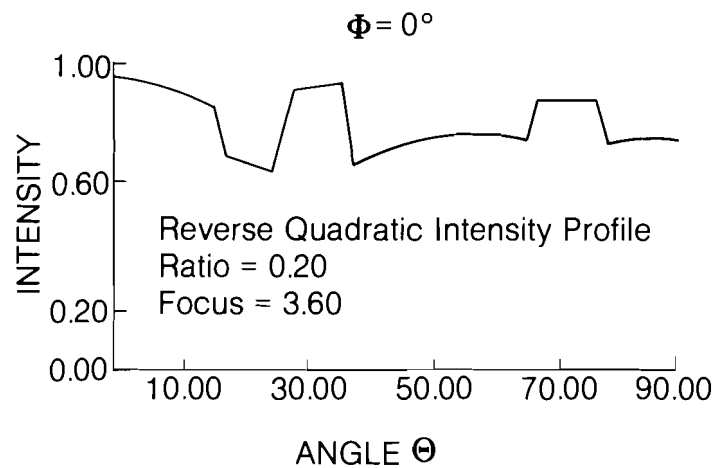


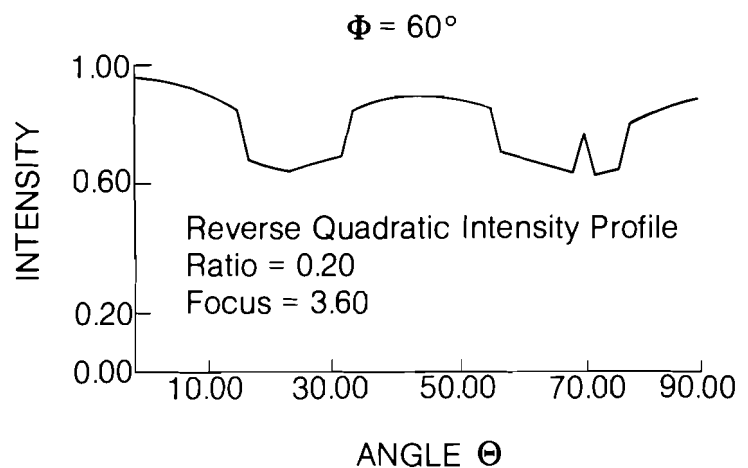
Figure 11
 Intensity plot at constant longitude.

Figure 12
Intensity plot at constant longitude.



irradiated with beams having a reverse quadratic intensity radial profile (with depth to height ratio of 0.2). The focal position of each beam was varied for values 0.2, 3.6, and 5.6 target radii behind the target center for the OMEGA system. For the three cases shown, the established plasma scale length was of the order of $40 \mu\text{m}$, with an assumed total laser energy absorption of 45% (30% collisional absorption and 15% resonance absorption). An alternative representation of the intensity distribution on target is obtained by passing a plane through the intensity distribution at a constant latitude θ or longitude ϕ . Figure 11 is the $\phi = 0$ plot for beams focused 0.2 target radii behind the target center. Figures 12 and 13 are the corresponding $\phi = 0^\circ$ and $\phi = 60^\circ$ plots. Figures 14 and 15 show the $\theta = 40^\circ$ and $\theta = 85^\circ$ plots for beams focused 3.6 target radii behind target center. Similarly, Figures 16 through 19 are plots for beams focused 5.6 target radii behind target center. In order to model the effects of both "short" and "long" pulses proposed for experiments, the absorption coefficients for the processes we shall present here are for

Figure 13
Intensity plot at constant longitude.



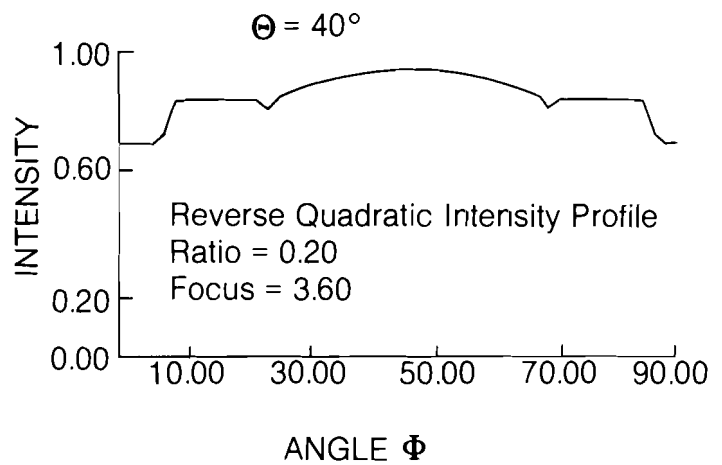


Figure 14
Intensity profile at constant latitude.

both “short” and “long” plasma layers (these layers are characterized by plasma scale lengths of 3 and 20 μm respectively) with:

1. A maximum amount of resonance absorption (up to 50% of the total absorption), and
2. A moderate amount of resonance absorption (up to 30% of the total absorption). The absorption coefficient is of the form: $A = aA_u + bA_v + cA_r$ where, a, b, and c are weight factors (constants). A_u includes all the absorption processes which are angularly independent (or weakly angularly dependent), such as ion acoustic turbulence^{15, 16}; A_v denotes the collisional processes proportional to $\cos^5\theta$ (inverse bremsstrahlung absorption for a ramp plasma profile)¹⁷; A_r represents the resonance absorption process where the functional fit of Forslund et al.¹⁸ has been used ($A_r = \xi \exp(1-2\xi)$ where $\xi = (2\pi L/\lambda)^{2/3} \sin^2\theta_0$ where θ_0 is the angle of incidence, L the plasma scale length, and λ the wavelength of the incident radiation).

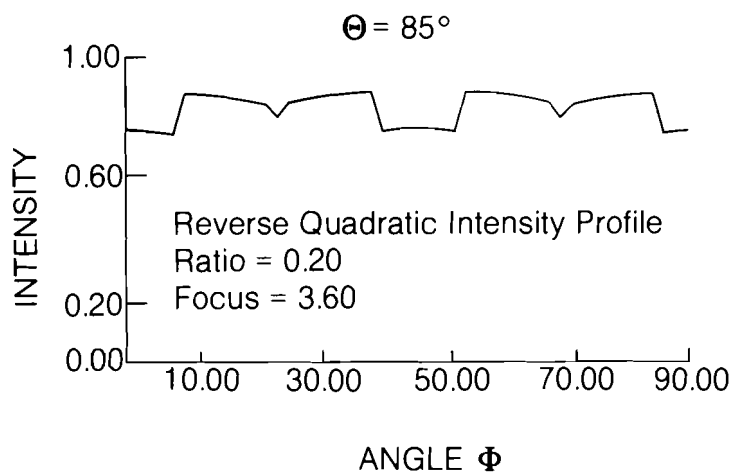


Figure 15
Intensity profile at constant latitude.

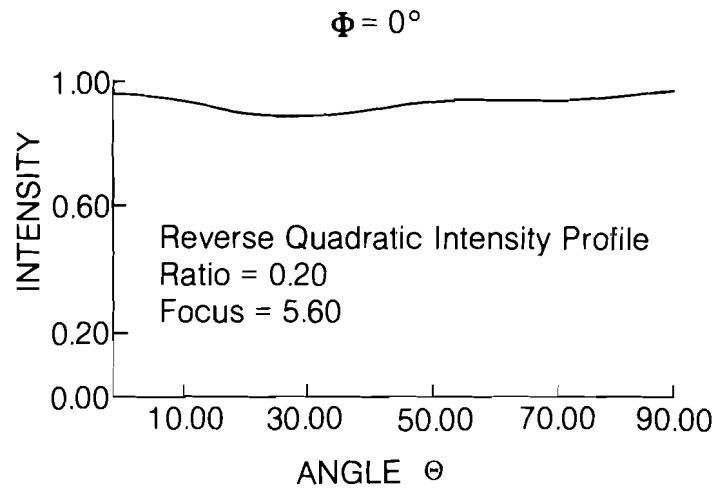


Figure 16
Intensity plot at constant longitude.

It should be pointed out that σ/\bar{I} versus focal position curves for experimentally observed absorption processes are expected to lie in the region bounded by these two limiting curves at or near the focal positions studied. Nevertheless, these limiting curves are slightly optimistic in nature due to the fact that neither diffraction nor nonlinear effects, such as self-focusing or filamentation, have been taken into consideration in the model.

For supergaussian and quadratic intensity profiles, the σ/\bar{I} versus focal position curves (for both models employing thick and thin plasma layers and assuming maximum resonance absorption) are seen to level off and approach 10% when the beams are focused more than 2.6 target radii behind the target center. Furthermore, the uniformity is seen to be quite sensitive to

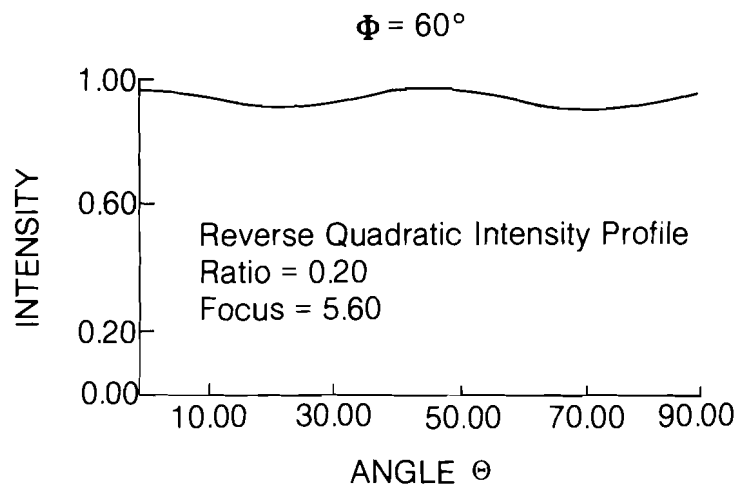


Figure 17
Intensity plot at constant longitude.

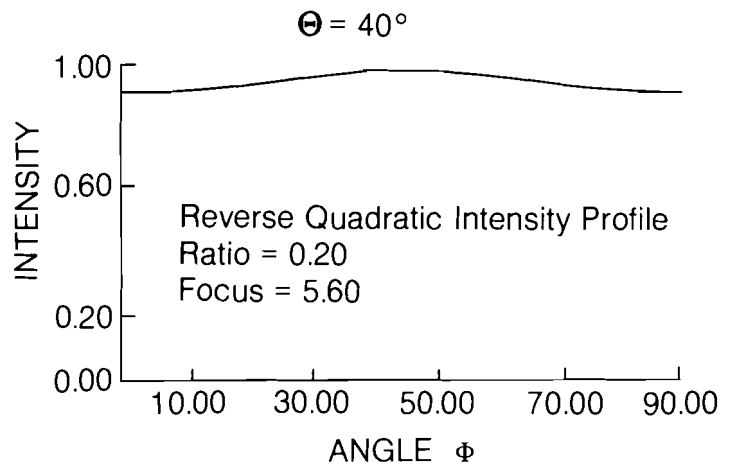


Figure 18
Intensity profile at constant latitude.

target misalignment. Thus, from the standpoint of uniformity, both quadratic and supergaussian intensity profiles are not very suitable for target illumination for the ZETA subsystem of OMEGA.

For the flat top and reverse quadratic intensity profiles, the σ/\bar{I} versus focal position curves for all absorption coefficients and all simulated intensity profiles are seen to have a relative minimum below 10% for different focal positions (Figure 20). Moreover, the curves for each absorption coefficient have the same qualitative features for different intensity profiles in this category. We have also found that even for different mixtures of various absorption processes, the curves lie close to one another. These results hold for both "long" and "short" plasma layers. Furthermore, the uniformity is less sensitive to misalignment errors compared to

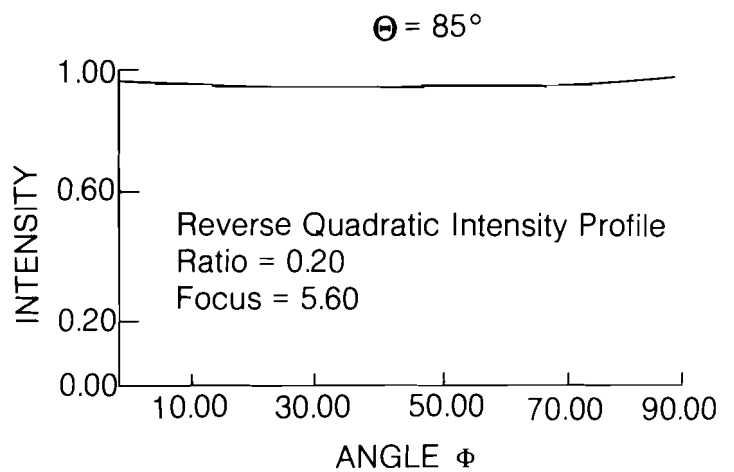


Figure 19
Intensity profile at constant latitude.

that seen for the supergaussian or quadratic radial beam profile models. Nonuniformity (σ/\bar{I}) remains below 10% for target displacements from the chamber center for target position errors as large as 0.25 target radii.

The best focal position for each beam depends on the absorption processes taking place. Our simulations show that independent of the details of our model absorption processes and beam radial intensity profiles studied, the beam should be focused at or beyond 2.1 target radii behind the target center.

Recent experimental results with the ZETA system have verified these theoretical results and exhibit the same qualitative behavior¹⁹ as our model curves. For the focal position at a distance b less than one target radius R behind the target center, considerable absorption nonuniformity has been observed. The experiments show that a steady improvement in uniformity is observed as b increases up to $2.7R$, where the uniformity is quite satisfactory.

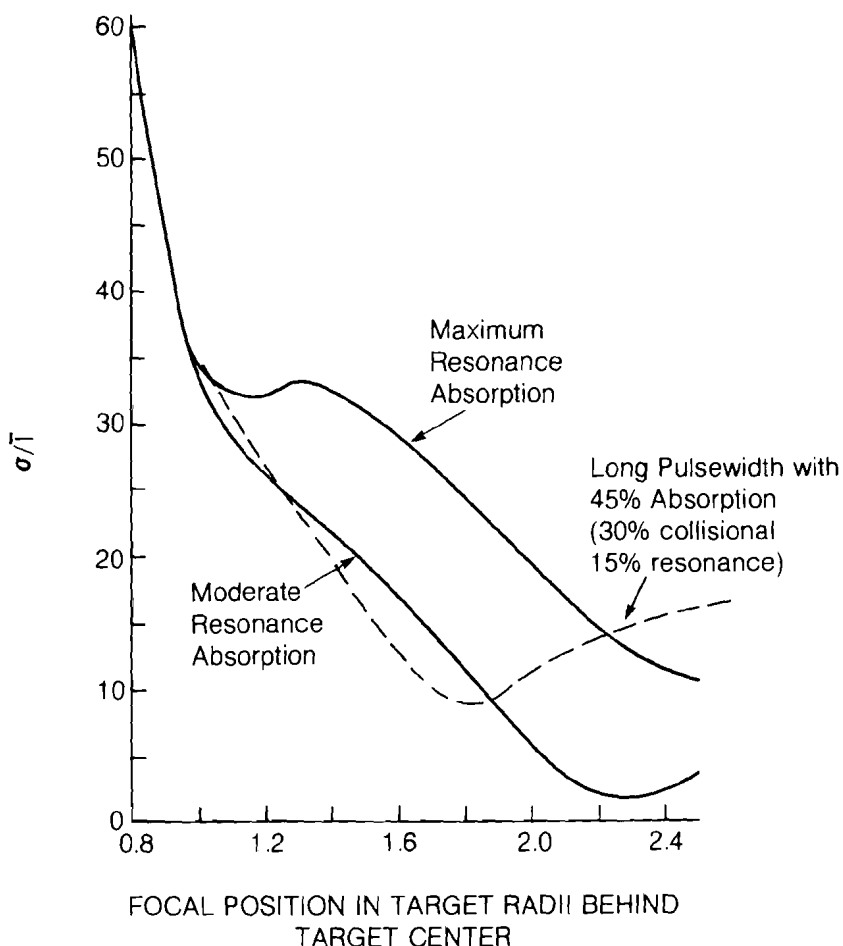
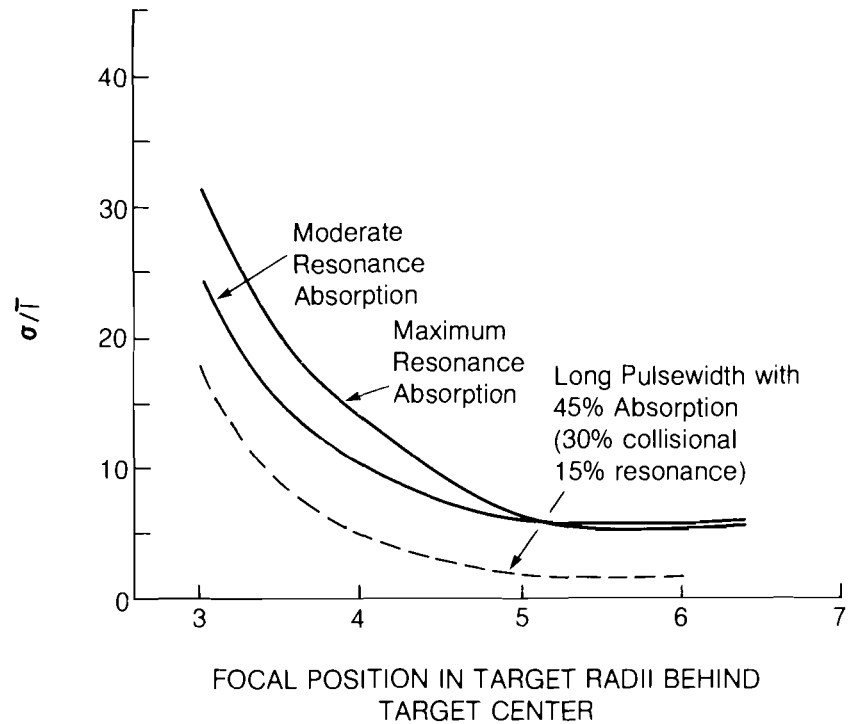


Figure 20
 σ/\bar{I} versus focal position ZETA
 with reverse quadratic intensity
 profile (depth to height ratio of
 0.2).

Figure 21
 σ/\bar{I} versus focal position for OMEGA
 with reverse quadratic intensity
 profile (depth to height ratio of
 0.2).



Uniformity of illumination is expected to improve for the full OMEGA laser system over that of the ZETA subsystem due to an increase in the number of symmetrically arranged laser beams. Our numerical simulations of target illumination for the OMEGA system have confirmed that this is indeed the case. The curves for both “long” and “short” plasma scalelengths are clustered together. Furthermore, independent of the assumed beam radial intensity profiles, the curves asymptotically approach the 6% line (Figure 21). We conclude that if the beams are focused at or beyond 5.4 target radii behind the target center, nonuniformity of the illumination of 6% or less will be achieved on target. Moreover, the uniformity of illumination was found to be quite insensitive to reasonable target centering errors.

Alternate designs with different lens $f/\#$ for both the ZETA and OMEGA systems have been considered. The qualitative features of σ/\bar{I} versus focal position curves are similar to the original designs, differing only in the optimal focal position and the minimum value of σ/\bar{I} .

In summary, a nonuniformity (σ/\bar{I}) of 10% or less can be achieved for the ZETA system, provided the radial beam intensity profiles are neither like the supergaussian nor quadratic profiles, and 6% or less nonuniformity can be attained for the OMEGA system. Long pulsewidth simulations, corresponding to an established plasma scalelength on the order of 40 μm have

recently been considered for both the ZETA and OMEGA systems. The total laser energy absorption for the long pulsewidth case is assumed to be 45% (partitioned as 30% collisional absorption and 15% resonance absorption). These simulation results show that the use of long pulsewidth laser pulses on the ZETA system results in nonuniformity of illumination similar to those obtained in the short pulse research. However, simulations of long pulsewidth pulses on the full OMEGA system result in nonuniformity of illumination of order less than 3% for the model beam profiles considered.

At present, the following improvements to our computer simulation of illumination uniformity are being considered:

1. to include scalar diffraction effects,
2. to model absorption coefficients in a more self-consistent way,
3. to calculate uniformity effects using measured beam radial intensity profiles in contrast with the model profiles we have described here, and
4. to model the effects of system energy imbalance.